Available online at www.sciencedirect.com
SCIENCE DIRECT
Journal of Sound and Vibration 294 (2006) 1073–1093
JOURNAL OF SOUND AND VIBRATION
www.elsevier.com/locate/jsvi

On the symmetric modal interaction of the suspended cable: Three-to-one internal resonance

Yueyu Zhao, Lianhua Wang*

College of Civil Engineering, Hunan University, Changsha, Hunan 410082, PR China

Received 8 October 2004; received in revised form 27 July 2005; accepted 7 January 2006
Available online 9 March 2006

Abstract

The two-mode nonlinear response of a suspended cable subjected to the primary resonance is investigated, and the three-to-one internal resonance is analyzed. Because the treatment of Galerkin discrete models of spatially continuous systems with initial curvature may lead to erroneous quantitative or even qualitative results, the method of multiple scales is applied to directly attack the nonlinear partial differential equation and the boundary conditions, which leads to the modulation equations for the primary resonance of either the first or third symmetric mode. The Newton–Raphson method and the pseudo-arclength scheme are used to obtain the frequency-response curves and force-response curves, and the dynamic solutions of the modulation equations are also investigated.

1. Introduction

The long-span cable structures are widely used in several engineering fields, such as voltage transmission lines, cable-supported bridges, mooring cables [1]. Because of their practical significance, various aspects of the dynamics of cables have already been investigated. Irvine and Caughey [2] developed the linear dynamics of elastic cables with a small sag, and a general review of the linear vibration of an elastic cable can be found in Ref. [3]. Using the single-degree-of-freedom (sdof) cable model, many researchers have investigated the finite free and forced oscillation of elastic cables [4–6], and found many interesting nonlinear phenomena because of the presence of both quadratic and cubic nonlinearities. Moreover, many interaction phenomena may also occur due to the internal resonance, and the previous works about the modal interactions in the cable structure related to the current investigation are presented as follows.

In order to understand the energy exchange in the Hamiltonian case, Benedettini et al. [7] investigated the modal coupling between in-plane and out-plane motions by using a discrete model. Rao et al. [8] studied the nonlinear response of a suspended cable under periodic excitation. In their study, the two-to-one internal resonance between the symmetric in-plane mode and out-of-plane vibration was investigated by using the two-degree-of-freedom model, and they found that the nonplanar motion of a cable with a given sag may be activated within a certain region of the external resonance. Perkins [9] examined the effect of one support

*Corresponding author.
E-mail address: wanglianhua1975@yahoo.com (L. Wang).

0022-460X/$ - see front matter © 2006 Elsevier Ltd. All rights reserved.
doi:10.1016/j.jsv.2006.01.004

motion on the three-dimensional nonlinear response. Using the Galerkin method, he constructed a two-degree-of-freedom model to analyze the two-to-one internal resonance, and the method of multiple scales was applied to the first-order perturbation analysis of the discretized model. Lee and Perkins [10] extended the study to the second-order perturbation, but their study still focused on the two-to-one internal resonance. By using a three-degree-of-freedom model, Lee and Perkins [11] found that strong coupling between in-plane and out-of-plane components occurred under simultaneous one-to-one internal resonance and two-to-one internal resonance. Pakdemirli et al. [12] investigated the one-to-one internal resonance between the second symmetric in-plane and out-of-plane modes of a suspended cable, and they found that the frequency-response curves of the two modes depended on the discretization or the direct method. Benedettini et al. [13] examined the nonlinear response of the suspended cable by using the method of multiple scales to treat the four-degree-of-freedom discretized model near the first *crossover* point.

Using the experimental method, Rega et al. [14] investigated the nonlinear dynamics of a suspended cable with the cable parameters corresponding to the first *crossover* point, and they observed strong nonlinear interaction phenomena among different contributing modes. By directly attacking the integral-partial-differential equations governing the nonlinear vibrations of suspended cables, Rega et al. [15] showed that the treatment of the four-degree-of-freedom discretized model might lead to erroneous results. Nayfeh et al. [16] made another study on the same model by directly attacking the equations of motion by the method of multiple scales, and they observed complex nonlinear response and a sequence of period-doubling bifurcations. Zhao et al. [17] examined the coupling dynamics of inclined cables between in-plane and out-of-plane vibrations under one-to-one internal resonances. Recently, based on the 3-D model formulation, which is not restricted to cables with very small sag, Srinil et al. [18] investigated the nonlinear characteristics of the large amplitude free vibrations of inclined sagged cables. And they observed strong coupling phenomena when the two-to-one internal resonance conditions were activated.

All the above studies only focused on one-to-one or two-to-one internal resonances, and little research was related to three-to-one internal resonances in suspended cables. In this aspect, we only found that Lacarbonara et al. [19] presented a detailed picture of activation/orthogonality of bimodal interactions in suspended cables, and their results showed that three-to-one internal resonances might be activated between the symmetric modes.

The object of this study is to investigate the nonlinear response of suspended homogeneous elastic cables with small initial sag-to-span ratios in the case of three-to-one internal resonances, subjected to the vertical load. This paper is organized as follows. In Section 2, we first present the nondimensional equation of in-plane motion. Then we consider the relation between the natural frequencies and the elasto-geometric parameter [20], which shows that there may exist three-to-one internal resonances between the symmetric modes. In Section 3, the method of multiple scales is applied to the equation of motion and boundary conditions to obtain the modulation equations for the primary resonance of the first and third symmetric mode. Section 4 presents the equilibrium solutions of the modulation equations for the primary resonances. And the dynamic solutions of the modulation equations for the primary resonances are investigated in Section 5. A short summary of the results is presented in Section 6.

2. Problem formulation

Considering a suspended homogenous elastic cable whose two supports are fixed, the suspended cable is subjected to a distributed harmonic excitation, as shown in Fig. 1. Neglecting the bending, torsional and shear rigidities, and assuming that the suspended cable stretches in a *quasi-static* manner [9] due to the fact that the transverse wave speed is much lower than the longitudinal wave speed, the nondimensional equation governing the nonlinear in-plane motion of the suspended cable can be expressed by the following partial differential equation [13,16]:

$$\ddot{w} + 2c\dot{w} - w'' - \alpha(w'' + y'') \int_0^1 \left\{ y'w' + \frac{1}{2} w'^2 \right\} \mathrm{d}x = F(x)\cos(\Omega t). \tag{1}$$

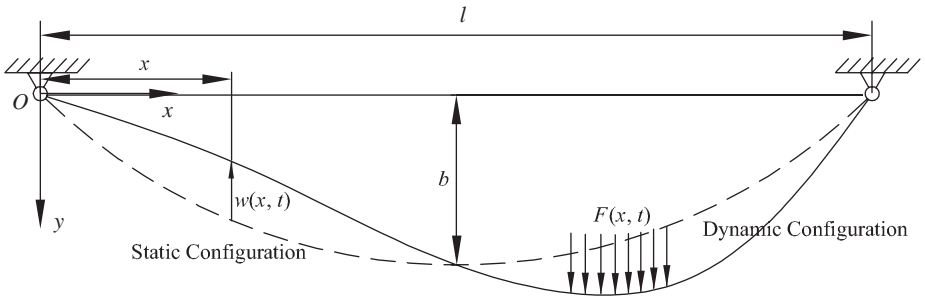

Fig. 1. The suspended cable's configurations.

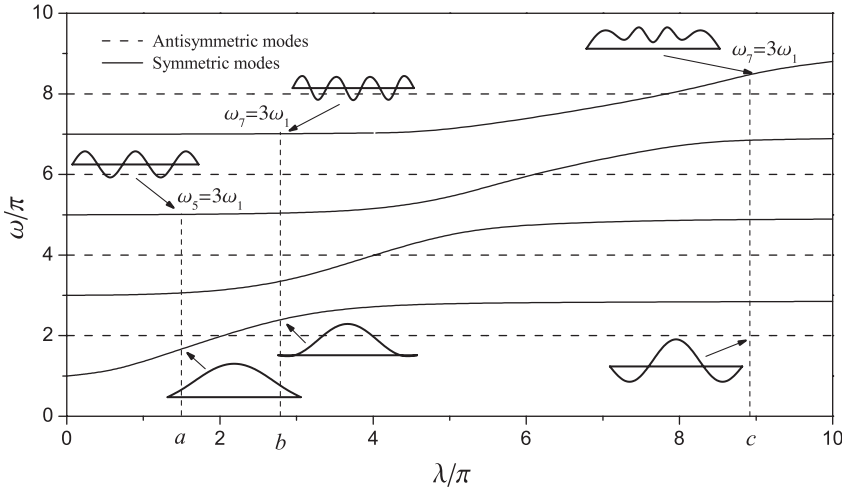

Fig. 2. Variations of the nondimensional natural frequencies with λ/π.

The boundary conditions are given by

$$w(x,t) = 0, \quad \text{at } x = 0 \text{ and } x = 1. \tag{2}$$

In Eq. (1), $y(x) = 4fx(1-x)$ is the initial parabolic shape of the suspended cable; $f = b/l$ is the sag-to-span ratio; b is the cable sag; l is the span of the cable; $\alpha = EA/H = 8bEA/(mgl)$ is the nondimensional stiffness parameter [19]; m is the mass per unit length; E is the Young modulus; A is the area of the cross section; g is the gravitational acceleration; c is the nondimensional damping coefficients; w is the in-plane displacement (nondimensionalized with respect to the span); the overdot indicates the differentiation with respect to the nondimensional time t; the prime indicates the differentiation with respect to the nondimensional coordinate x; $F(x)$ describes the spatial distribution of the harmonic load; and Ω is the nondimensional frequency of the harmonic load.

The symmetric in-plane eigenmodes are given by

$$\phi_i(x) = c_i[1 - \tan(\tfrac{1}{2}\omega_i)\sin\omega_i x - \cos\omega_i x], \quad i = 1, 3, 5, \ldots, \tag{3}$$

where c_i are chosen so that the modes satisfy the orthonormality condition. And the eigenfrequencies are determined by

$$\frac{1}{2}\omega_i - \tan\left(\frac{\omega_i}{2}\right) - \frac{1}{2\lambda^2}\omega_i^3 = 0, \tag{4}$$

where $\lambda^2 = EA/mgl(8b/l)^3$. The antisymmetric in-plane eigenmodes and eigenfrequencies are given by

$$\phi_i(x) = \sqrt{2}\sin i\pi x, \quad \omega_i = i\pi, \quad i = 2,4,6,\ldots. \tag{5}$$

The variations of the eight lowest calculated nondimensional natural frequencies with the elasto-geometric parameter λ are shown in Fig. 2. The obtained natural frequencies are the same as those of Lacarbonara et al. [19], and we can note that the three-to-one internal resonance between the symmetric in-plane modes is possible for a certain range of λ/π. For example, the three-to-one internal resonance between the third and first symmetric modes may be activated when λ is close to $a \approx 1.51\pi$, and the three-to-one internal resonance between the fourth and first symmetric modes may be activated when λ is close to $b \approx 2.55\pi$ or $c \approx 8.91\pi$. Lacarbonara et al. [19] pointed out the latter two cases. However, the first case seemed to be ignored. Moreover, the three-to-one internal resonances between the symmetric modes and antisymmetric or nonplanar modes are not activable because the nonlinear interaction terms equal to zero [19].

Because the discretization would lead to erroneous results for systems with quadratic and cubic nonlinearities [15,21], we use the method of multiple scales to directly attack the nonlinear equation of motion and boundary conditions to investigate the three-to-one internal resonance between the third and first symmetric mode in the following section.

3. Perturbation analysis

Lacarbonara et al. [22] have obtained the general modulation equations related to three-to-one internal resonances in nonlinear continuous systems with linear, quadratic, and cubic geometric operators by directly applying the method of multiple scales to the governing equations of motion and boundary conditions. Similarly, following Lacarbonara et al. [22], we use the method of multiple scales to obtain the modulation equations governing the nonlinear dynamic of suspended cables in the case of three-to-one internal resonances. First, we rewrite Eq. (1) as a system of two first-order equations in time as follows:

$$\dot{w} - u = 0, \tag{6}$$

$$\dot{u} + 2cu - w'' - \alpha(w'' + y'')\int_0^1 \left\{ w'y' + \frac{1}{2}w'^2 \right\} \mathrm{d}x = F(x)\cos(\Omega t). \tag{7}$$

Because the resonant terms appear at the third order [22], we can seek uniform expansions of w and u in the following form:

$$u(x,t) = \sum_{i=1}^{3} \varepsilon^i u_i(x, T_0, T_2) + \cdots, \tag{8}$$

$$w(x,t) = \sum_{i=1}^{3} \varepsilon^i w_i(x, T_0, T_2) + \cdots, \tag{9}$$

where $T_i = \varepsilon^i t$, where ε is a small bookkeeping parameter. In order to let the damping, nonlinearity and resonance balance each other, we rescale c and F as $c \to \varepsilon^2 c$ and $F \to \varepsilon^3 F$. Substituting Eqs. (8) and (9) into Eqs. (6) and (7), and equating the coefficients of like powers of ε, we can obtain:

Order ε:

$$D_0 w_1 - u_1 = 0, \tag{10}$$

$$D_0 u_1 - w_1'' - \alpha y'' \int_0^1 w_1' y' \,\mathrm{d}x = 0, \tag{11}$$

Order ε^2:

$$D_0 w_2 - u_2 = 0, \tag{12}$$

$$D_0u_2 - w_2'' - \alpha y'' \int_0^1 w_2' y' \,\mathrm{d}x = \alpha w_1'' \int_0^1 y' w_1' \,\mathrm{d}x + \frac{1}{2}\alpha y'' \int_0^1 w_1' w_1' \,\mathrm{d}x, \tag{13}$$

Order ε^3:

$$D_0w_3 - u_3 = -D_2w_1 - D_1w_2, \tag{14}$$

$$\begin{aligned} D_0u_3 - w_3'' - \alpha y'' \int_0^1 w_2' y' \,\mathrm{d}x = & -D_2u_1 - D_1u_2 - 2cu_1 \\ & + \alpha w_1'' \int_0^1 y' w_2' \,\mathrm{d}x + \alpha w_2'' \int_0^1 y' w_1' \,\mathrm{d}x + \alpha y'' \int_0^1 w_1' w_2' \,\mathrm{d}x \\ & + \frac{1}{2}\alpha w_1'' \int_0^1 w_1' w_1' \,\mathrm{d}x + F\cos\Omega T_0, \end{aligned} \tag{15}$$

where $D_i = \partial/\partial T_i$. The boundary conditions are given by

$$w_i = 0, \quad u_i = 0 \ \text{ at } x = 0 \quad \text{and} \quad x = 1 \ \text{ for } i = 1, 2, 3. \tag{16}$$

Because all the modes that are not directly or indirectly excited die out after a long time due to the damping effect [23], the solution of the first-order problem is assumed to consist of the first and third symmetric modes; that is

$$w_1 = A_1(T_2)\phi_1(x)\mathrm{e}^{\mathrm{i}\omega_1 T_0} + A_3(T_2)\phi_3(x)\mathrm{e}^{\mathrm{i}\omega_3 T_0} + \mathrm{cc}, \tag{17}$$

$$u_1 = \mathrm{i}\omega_1 A_1(T_2)\phi_1(x)\mathrm{e}^{\mathrm{i}\omega_1 T_0} + \mathrm{i}\omega_3 A_3(T_2)\phi_3(x)\mathrm{e}^{\mathrm{i}\omega_3 T_0} + \mathrm{cc}, \tag{18}$$

where $\phi_i(x)$ and ω_i are the ith symmetric mode and corresponding frequency, cc stands for the complex conjugate of the preceding terms, and the complex-valued functions $A_3(T_2)$ and $A_1(T_2)$ are determined by imposing the solvability conditions at the third order. Substituting Eqs. (17) and (18) into Eqs. (12) and (13), we can obtain

$$D_0w_2 - u_2 = 0, \tag{19}$$

$$\begin{aligned} D_0u_2 - w_2'' - \alpha y'' \int_0^1 w_2' y' \,\mathrm{d}x = & A_1^2\mathrm{e}^{2\mathrm{i}\omega_1 T_0}\Pi_1 + A_3^2\mathrm{e}^{2\mathrm{i}\omega_3 T_0}\Pi_2 + A_1A_3\mathrm{e}^{\mathrm{i}(\omega_3+\omega_1)T_0}\Pi_3 \\ & + A_3\bar{A}_1\mathrm{e}^{\mathrm{i}(\omega_3-\omega_1)T_0}\Pi_4 + A_1\bar{A}_1\Pi_5 + A_3\bar{A}_3\Pi_6 + \mathrm{cc}, \end{aligned} \tag{20}$$

where Π_i are defined in Appendix A. Then the solutions of Eqs. (19)–(20) can be written as follows:

$$\begin{aligned} w_2 = & A_1^2\mathrm{e}^{2\mathrm{i}\omega_1 T_0}\Psi_1(x) + A_3^2\mathrm{e}^{2\mathrm{i}\omega_3 T_0}\Psi_2(x) + A_3A_1\mathrm{e}^{\mathrm{i}(\omega_1+\omega_3)T_0}\Psi_3(x) \\ & + A_3\bar{A}_1\mathrm{e}^{\mathrm{i}(\omega_3-\omega_1)T_0}\Psi_4(x) + A_1\bar{A}_1\Psi_5(x) + A_3\bar{A}_3\Psi_6(x) + \mathrm{cc}, \end{aligned} \tag{21}$$

$$\begin{aligned} u_2 = & A_1^2\mathrm{e}^{2\mathrm{i}\omega_1 T_0}\psi_1(x) + A_3^2\mathrm{e}^{2\mathrm{i}\omega_3 T_0}\psi_2(x) + A_3A_1\mathrm{e}^{\mathrm{i}(\omega_1+\omega_3)T_0}\psi_3(x) \\ & + A_3\bar{A}_1\mathrm{e}^{\mathrm{i}(\omega_3-\omega_1)T_0}\psi_4(x) + A_1\bar{A}_1\psi_5(x) + A_3\bar{A}_3\psi_6(x) + \mathrm{cc}, \end{aligned} \tag{22}$$

where the second-order shape functions $\Psi_i(x)$ ($i = 1, 2, 3, 4, 5, 6$) are the solutions of the following boundary-value problem:

$$\Psi_1'' + \alpha y'' \int_0^1 \Psi_1' y' \,\mathrm{d}x + 4\omega_1^2\Psi_1 = -\Pi_1, \tag{23}$$

$$\Psi_2'' + \alpha y'' \int_0^1 \Psi_2' y' \,\mathrm{d}x + 4\omega_3^2\Psi_2 = -\Pi_2, \tag{24}$$

$$\Psi_3'' + \alpha y'' \int_0^1 \Psi_3' y' \,\mathrm{d}x + (\omega_3 + \omega_1)^2\Psi_3 = -\Pi_3, \tag{25}$$

$$\Psi_4'' + \alpha y'' \int_0^1 \Psi_4' y' \,\mathrm{d}x + (\omega_3 - \omega_1)^2 \Psi_4 = -\Pi_4, \tag{26}$$

$$\Psi_5'' + \alpha y'' \int_0^1 \Psi_5' y' \,\mathrm{d}x = -\Pi_5, \tag{27}$$

$$\Psi_6'' + \alpha y'' \int_0^1 \Psi_6' y' \,\mathrm{d}x = -\Pi_6, \tag{28}$$

with all of the functions satisfying the boundary conditions. On the other hand, the functions associated with the second-order velocity field are given by

$$\psi_1(x) = 2\mathrm{i}\omega_1 \Psi_1(x), \quad \psi_2(x) = 2\mathrm{i}\omega_3 \Psi_2(x), \quad \psi_3(x) = \mathrm{i}(\omega_3 + \omega_1)\Psi_3(x),$$

$$\psi_4(x) = \mathrm{i}(\omega_3 - \omega_1)\Psi_4(x), \quad \psi_5(x) = 0, \quad \psi_6(x) = 0. \tag{29}$$

Substituting Eqs. (17), (18), (21), (22) into the third-order Eqs. (14) and (15), we can obtain

$$D_0 w_3 - u_3 = -D_2 A_1 \mathrm{e}^{\mathrm{i}\omega_1 T_0}\phi_1 - D_2 A_3 \mathrm{e}^{\mathrm{i}\omega_3 T_0}\phi_3 + \mathrm{cc} + \mathrm{NST}, \tag{30}$$

$$\begin{aligned} D_0 u_3 - w_3'' - \alpha y'' \int_0^1 y' w_3' \,\mathrm{d}x = & -\mathrm{i}\omega_1 (D_2 A_1 + 2cA_1)\mathrm{e}^{\mathrm{i}\omega_1 T_0}\phi_1 - \mathrm{i}\omega_1 (D_2 A_3 + 2cA_3)\mathrm{e}^{\mathrm{i}\omega_3 T_0}\phi_3 \\ & + \chi_1(x) A_1^2 \bar{A}_1 \mathrm{e}^{\mathrm{i}\omega_1 T_0} + \chi_2(x) A_1 A_3 \bar{A}_3 \mathrm{e}^{\mathrm{i}\omega_1 T_0} + \chi_3(x) A_3 \bar{A}_1 \bar{A}_1 \mathrm{e}^{\mathrm{i}(\omega_3 - 2\omega_1)T_0} \\ & + \chi_4(x) A_3 A_1 \bar{A}_1 \mathrm{e}^{\mathrm{i}\omega_3 T_0} + \chi_5(x) A_3^2 \bar{A}_3 \mathrm{e}^{\mathrm{i}\omega_3 T_0} + \chi_6(x) A_1^3 \mathrm{e}^{3\mathrm{i}\omega_1 T_0} + \frac{F}{2}\mathrm{e}^{\mathrm{i}\Omega T_0} \\ & + \mathrm{cc} + \mathrm{NST}, \end{aligned} \tag{31}$$

where NST stands for the terms that do not produce secular effects, and $\chi_i(x)$ are defined in Appendix A.

To describe the nearness of ω_3 to $3\omega_1$ and Ω to either ω_1 or ω_3, we introduce the detuning parameters σ_1 and σ_2 defined as

$$\omega_3 = 3\omega_1 + \varepsilon^2 \sigma_1 \quad \text{and} \quad \Omega = \omega_i + \varepsilon^2 \sigma_2, \quad i = 1, 3. \tag{32}$$

Because the homogeneous problems governing w_3 and u_3 admit nontrivial solutions, the corresponding nonhomogeneous problem has a solution only if the solvability conditions are satisfied. In this case, the right-hand side of Eqs. (30) and (31) need to be orthogonal to every solution of the adjoint problem. Therefore, we can obtain the following solvability conditions:

$$2\mathrm{i}\omega_1 (A_1' + \mu_1 A_1) = \Gamma_{11} A_1^2 \bar{A}_1 + \Gamma_{12} A_1 A_3 \bar{A}_3 + \Gamma_{13} A_3 \bar{A}_1^2 \mathrm{e}^{\mathrm{i}\sigma_1 T_2} + \frac{f_1}{2}\delta_{i1}\mathrm{e}^{\mathrm{i}\sigma_2 T_2}, \tag{33}$$

$$2\mathrm{i}\omega_3 (A_3' + \mu_2 A_3) = \Gamma_{21} A_3 A_1 \bar{A}_1 + \Gamma_{22} A_3^2 \bar{A}_3 + \Gamma_{23} A_1^3 \mathrm{e}^{-\mathrm{i}\sigma_1 T_2} + \frac{f_3}{2}\delta_{i3}\mathrm{e}^{\mathrm{i}\sigma_2 T_2}, \tag{34}$$

where Γ_{ij}, μ_i, f_1, f_3 are defined in Appendix A, δ is the Kronecker delta, and the prime indicates the derivative with respect to T_2. We note that, except for the damping terms, the system is conservative and hence must be derivable from the Lagrangian [21]:

$$\begin{aligned} L = & \mathrm{i}\omega_1 (A_1 \bar{A}_1' - A_1' \bar{A}_1) + \mathrm{i}\omega_3 (A_3 \bar{A}_3' - A_3' \bar{A}_3) + \frac{1}{2}\Gamma_{11} A_1^2 \bar{A}_1^2 + \frac{1}{2}\Gamma_{22} A_3^2 \bar{A}_3^2 \\ & + \Gamma_{12} A_3 A_1 \bar{A}_3 \bar{A}_1 + \frac{f_1}{2}\delta_{i1}\bar{A}_1 \mathrm{e}^{\mathrm{i}\sigma_2 T_2} + \frac{f_1}{2}\delta_{i1} A_1 \mathrm{e}^{-\mathrm{i}\sigma_2 T_2} + \frac{f_3}{2}\delta_{i3}\bar{A}_3 \mathrm{e}^{\mathrm{i}\sigma_2 T_2} + \frac{f_3}{2}\delta_{i3} A_3 \mathrm{e}^{-\mathrm{i}\sigma_2 T_2}. \end{aligned} \tag{35}$$

Consequently,

$$\Gamma_{12} = \Gamma_{21} \quad \text{and} \quad \Gamma_{13} = 3\Gamma_{23}. \tag{36}$$

Next, we consider the primary resonance of the first and third symmetric mode separately.

3.1. Primary resonance of the first symmetric mode

Introducing the following polar transformation:

$$A_j = \tfrac{1}{2} a_j e^{i\beta_j}, \quad j = 1, 3, \tag{37}$$

substituting Eq. (37) into Eqs. (33) and (34), and separating the real and imaginary parts, we can obtain the following polar form of the modulation equations:

$$a_1' = -\mu_1 a_1 + \frac{\Gamma_{13}}{8\omega_1} a_1^2 a_3 \sin\gamma_1 + \frac{f_1}{2\omega_1} \sin\gamma_2, \tag{38}$$

$$a_3' = -\mu_2 a_3 - \frac{\Gamma_{23}}{8\omega_3} a_1^3 \sin\gamma_1, \tag{39}$$

$$a_1\beta_1' = -\frac{\Gamma_{11}}{8\omega_1} a_1^3 - \frac{\Gamma_{12}}{8\omega_1} a_3^2 a_1 - \frac{\Gamma_{13}}{8\omega_1} a_1^2 a_3 \cos\gamma_1 - \frac{f_1}{2\omega_1} \cos\gamma_2, \tag{40}$$

$$a_3\beta_3' = -\frac{\Gamma_{21}}{8\omega_3} a_1^2 a_3 - \frac{\Gamma_{22}}{8\omega_3} a_3^3 - \frac{\Gamma_{23}}{8\omega_3} a_1^3 \cos\gamma_1, \tag{41}$$

where

$$\gamma_1 = \beta_3 - 3\beta_1 + \sigma_1 T_2, \quad \gamma_2 = \sigma_2 T_2 - \beta_1. \tag{42}$$

Alternatively, we can express A_j in the following Cartesian form:

$$A_1 = \tfrac{1}{2}(p_1 - iq_1)e^{i\sigma_2 T_2} \quad \text{and} \quad A_3 = \tfrac{1}{2}(p_3 - iq_3)e^{i(3\sigma_2 - \sigma_1)T_2}. \tag{43}$$

Substituting Eq. (43) into Eqs. (33) and (34), and separating the real and imaginary parts, the following Cartesian form of the modulation equations can be obtained:

$$p_1' = -\mu_1 p_1 - \sigma_2 q_1 - \frac{1}{8\omega_1}\left\{\Gamma_{11} q_1 (p_1^2 + q_1^2) + \Gamma_{12} q_1 (p_3^2 + q_3^2)\right\} + \frac{\Gamma_{13}}{8\omega_1}\left\{q_3 (q_1^2 - p_1^2) + 2p_1 p_3 q_1\right\}, \tag{44}$$

$$q_1' = -\mu_1 q_1 + \sigma_2 p_1 + \frac{1}{8\omega_1}\left\{\Gamma_{11} p_1 (p_1^2 + q_1^2) + \Gamma_{12} p_1 (p_3^2 + q_3^2)\right\} + \frac{\Gamma_{13}}{8\omega_1}\left\{p_3 (p_1^2 - q_1^2) + 2p_1 q_1 q_3\right\} + \frac{f_1}{2\omega_1}, \tag{45}$$

$$p_3' = -\mu_2 p_3 - (3\sigma_2 - \sigma_1) q_3 - \frac{1}{8\omega_3}\left\{\Gamma_{21} q_3 (p_1^2 + q_1^2) + \Gamma_{22} q_3 (p_3^2 + q_3^2)\right\} - \frac{\Gamma_{23}}{8\omega_3}\left\{q_1 (3p_1^2 - q_1^2)\right\}, \tag{46}$$

$$q_3' = -\mu_2 q_3 + (3\sigma_2 - \sigma_1) p_3 + \frac{1}{8\omega_3}\left\{\Gamma_{21} p_3 (p_1^2 + q_1^2) + \Gamma_{22} p_3 (p_3^2 + q_3^2)\right\} - \frac{\Gamma_{23}}{8\omega_3}\left\{p_1 (3q_1^2 - p_1^2)\right\}. \tag{47}$$

Thus we can obtain the following second-order expansion of the nonlinear response of the suspended cable for the case of three-to-one resonance:

$$\begin{aligned} w(x,t) = {} & a_1 \cos(\Omega t - \gamma_2)\phi_1(x) + a_3 \cos(3\Omega t + \gamma_1 - 3\gamma_2)\phi_3(x) \\ & + \tfrac{1}{2}\{a_1^2[\cos 2(\Omega t - 2\gamma_2)\Psi_1(x) + \Psi_5(x)] + a_3^2[\cos 2(3\Omega t + \gamma_1 - 3\gamma_2)\Psi_2(x) + \Psi_6(x)] \\ & + a_1 a_3[\cos(4\Omega t + \gamma_1 - 4\gamma_2)\Psi_3(x) + \cos(2\Omega t + \gamma_1 - 2\gamma_2)\Psi_4(x)]\} + \cdots, \end{aligned} \tag{48}$$

where ε was set equal to one.

3.2. Primary resonance of the third symmetric mode

In this case, we can obtain the following polar form of the modulation equations:

$$a_1' = -\mu_1 a_1 + \frac{\Gamma_{13}}{8\omega_1} a_1^2 a_3 \sin\gamma_1, \tag{49}$$

$$a_3' = -\mu_2 a_3 - \frac{\Gamma_{23}}{8\omega_3} a_1^3 \sin\gamma_1 + \frac{f_3}{2\omega_3} \sin\gamma_2, \tag{50}$$

$$a_1\beta_1' = -\frac{\Gamma_{11}}{8\omega_1} a_1^3 - \frac{\Gamma_{12}}{8\omega_1} a_3^2 a_1 - \frac{\Gamma_{13}}{8\omega_1} a_1^2 a_3 \cos\gamma_1, \tag{51}$$

$$a_3\beta_3' = -\frac{\Gamma_{21}}{8\omega_3} a_1^2 a_3 - \frac{\Gamma_{22}}{8\omega_3} a_3^3 - \frac{\Gamma_{23}}{8\omega_3} a_1^3 \cos\gamma_1 - \frac{f_3}{2\omega_3} \cos\gamma_2, \tag{52}$$

where $\gamma_1 = \beta_3 - 3\beta_1 + \sigma_1 T_2$ and $\gamma_2 = \sigma_2 T_2 - \beta_3$. Similar, we can obtain the Cartesian form of the modulation equations:

$$p_1' = -\mu_1 p_1 - \frac{\sigma_1+\sigma_2}{3} q_1 - \frac{1}{8\omega_1}\left\{\Gamma_{11} q_1 (p_1^2+q_1^2) + \Gamma_{12} q_1 (p_3^2+q_3^2)\right\} + \frac{\Gamma_{13}}{8\omega_1}\left\{q_3(q_1^2-p_1^2) + 2p_1 p_3 q_1\right\}, \tag{53}$$

$$q_1' = -\mu_1 q_1 + \frac{\sigma_1+\sigma_2}{3} p_1 + \frac{1}{8\omega_1}\left\{\Gamma_{11} p_1 (p_1^2+q_1^2) + \Gamma_{12} p_1 (p_3^2+q_3^2)\right\} + \frac{\Gamma_{13}}{8\omega_1}\left\{p_3(p_1^2-q_1^2) + 2p_1 q_1 q_3\right\}, \tag{54}$$

$$p_3' = -\mu_2 p_3 - \sigma_2 q_3 - \frac{1}{8\omega_3}\left\{\Gamma_{21} q_3 (p_1^2+q_1^2) + \Gamma_{22} q_3 (p_3^2+q_3^2)\right\} - \frac{\Gamma_{23}}{8\omega_3}\left\{q_1(3p_1^2-q_1^2)\right\}, \tag{55}$$

$$q_3' = -\mu_2 q_3 + \sigma_2 p_3 - \frac{1}{8\omega_3}\left\{\Gamma_{21} p_3 (p_1^2+q_1^2) + \Gamma_{22} p_3 (p_3^2+q_3^2)\right\} - \frac{\Gamma_{23}}{8\omega_3}\left\{p_1(3q_1^2-p_1^2)\right\} + \frac{f_3}{2\omega_3}. \tag{56}$$

And the second-order expansion of the nonlinear response of the suspended cable is given by

$$\begin{aligned} w(x,t) = {} & a_1 \cos\left[\tfrac{1}{3}(\Omega t - \gamma_1 - \gamma_2)\right]\phi_1(x) + a_3 \cos(\Omega t - \gamma_2)\phi_3(x) \\ & + \tfrac{1}{2}\left\{a_1^2\left[\cos\tfrac{2}{3}(\Omega t - \gamma_1 - \gamma_2)\Psi_1(x) + \Psi_5(x)\right] + a_3^2[\cos 2(\Omega t - \gamma_2)\Psi_2(x) + \Psi_6(x)]\right. \\ & \left. + a_1 a_3\left[\cos(\tfrac{4}{3}\Omega t - \tfrac{1}{3}\gamma_1 - \tfrac{4}{3}\gamma_2)\Psi_3(x) + \cos(\tfrac{2}{3}\Omega t + \tfrac{1}{3}\gamma_1 - \tfrac{2}{3}\gamma_2)\Psi_4(x)\right]\right\} + \cdots. \end{aligned} \tag{57}$$

4. Equilibrium solutions

This section contains the details of the equilibrium solutions of the modulation equations for the chosen external and three-to-one internal resonance combination, where the excitation frequency is nearly equal to the natural frequency of the first and third symmetric mode. The coefficients of the modulation equations for three values of $\lambda(1.57\pi, 1.51\pi, 1.43\pi)$ are shown in Table 1, and the corresponding internal detuning parameter σ_1 is $-1.5, 0, 0.5$. And the six second-order shape functions Ψ_i are shown in Fig. 3, when $\lambda = 1.75\pi$. It may be noted that they are symmetric.

The equilibrium solution of the modulation equations corresponds to the periodic motion of the suspended cable. To determine the equilibrium solution, we can set $a_1' = a_3' = 0$ and $\gamma_1' = \gamma_2' = 0$ in the polar form of the modulation equations or set $p_1' = q_1' = p_3' = q_3' = 0$ in the Cartesian form of the modulation equations. In either case, the resulting systems of four nonlinear equations can be solved by using the Newton–Raphson method. We can note that the modulation equations only admit two-mode solution when the first symmetric mode is directly excited due to the presence of the term $\Gamma_{23} A_1^3 e^{-i\sigma_1 T_2}$ in Eq. (34). Whereas, the single-mode solution may occur when the third symmetric mode is directly excited due to the presence of the $\bar{A}$ in the third term of the right-hand side of Eq. (33).

Table 1
The nonlinear coefficients for different values of λ/π

λ/π	σ_1	Γ_{11}	Γ_{12}	Γ_{13}	Γ_{21}	Γ_{22}	Γ_{23}
1.75	−1.5	9.894×10^4	1.617×10^6	-9.621×10^4	1.617×10^6	-1.037×10^7	-3.207×10^4
1.51	0	6.507×10^4	1.306×10^6	-3.816×10^4	1.306×10^6	-1.019×10^7	-1.272×10^4
1.43	0.5	5.579×10^4	1.196×10^6	-2.882×10^4	1.196×10^6	-1.012×10^7	-0.960×10^4

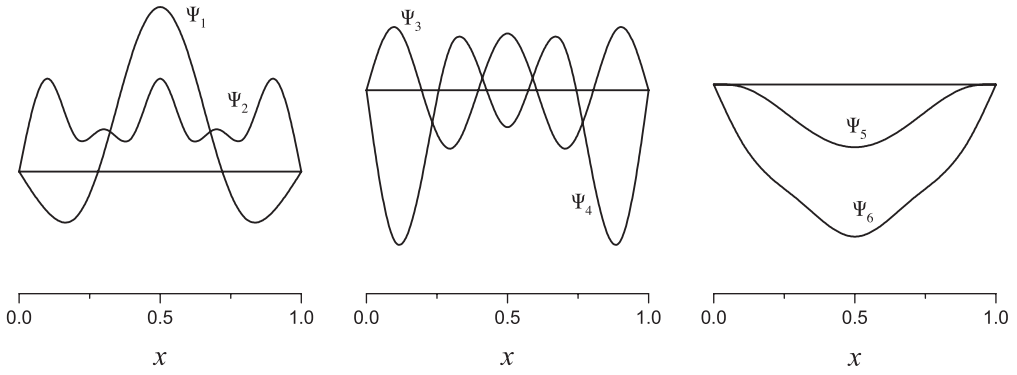

Fig. 3. The functions Ψ_i for the three-to-one internal resonance between the third and first symmetric mode when $\lambda = 1.75\pi$.

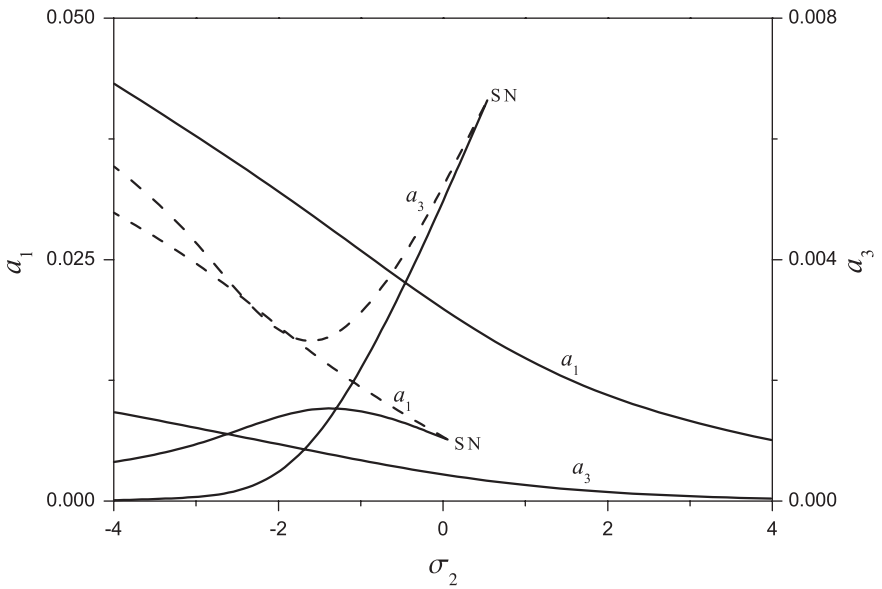

Fig. 4. Frequency-response curves for the primary resonance of the first symmetric mode: $\mu_1 = 0.05$, $\mu_2 = 0.01$, $f_1 = 0.16$ and $\sigma_1 = -1.5$.

After the equilibrium solution is determined, the stability of the equilibrium solution can then be assessed by applying the classical method of linearization [24]. Then, the pseudo-arclength path following algorithm [24] can be used to trace the solution branch. In the following frequency- or force-response curves, the stable and unstable solutions are indicated, respectively, by solid and dashed line.

4.1. Primary resonance of the first symmetric mode

Fig. 4 illustrates the amplitudes of the first and third symmetric mode as the functions of the detuning parameter σ_2 in the neighborhood of the primary resonance of the first symmetric mode with $\mu_1 = 0.05$, $\mu_2 = 0.01$, $f_1 = 0.16$, and $\sigma_1 = -1.5$, and SN represents the saddle-node point. The results shown in Fig. 4 exhibit a softening behavior for the frequency-response curves of the first symmetric mode, in which the quadratic nonlinearity due to the initial shape dominates the nonlinear response. This is mainly due to the fact that the coefficient Γ_{11} is positive. Fig. 4 also shows that the modulation equations have two stable solutions and one unstable solution when $\sigma_2 < 0.157$. And the initial conditions determine which stable solution the suspended cable's response settles. Whereas, the unstable solution does not exist in the suspended cable's response.

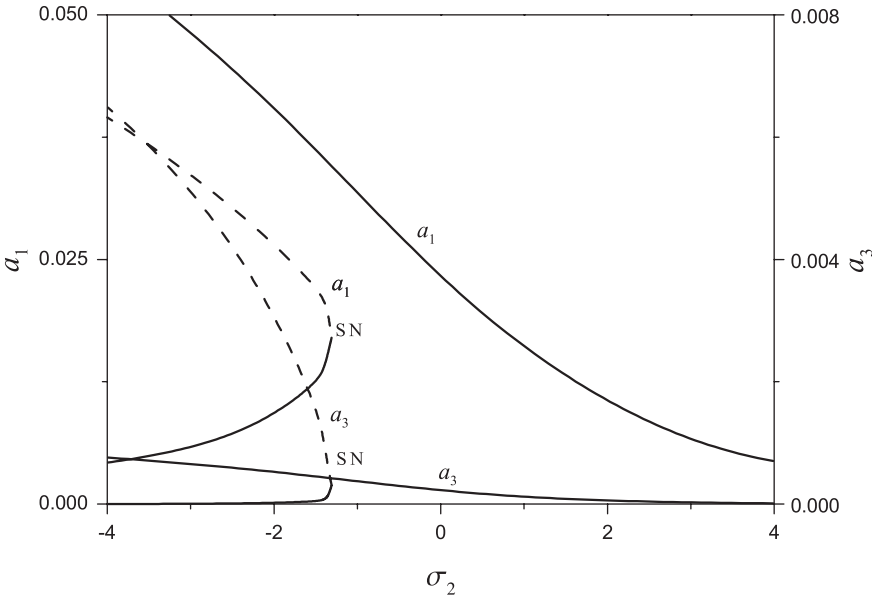

Fig. 5. Frequency-response curves for the primary resonance of the first symmetric mode: $\mu_1 = 0.05$, $\mu_2 = 0.01$, $f_1 = 0.16$ and $\sigma_1 = 0.5$.

As the detuning parameter σ_2 increases from a very small value, the lower stable solution of the first symmetric mode grows first, then decreases until a saddle-node bifurcation occurs at SN, where one of the corresponding eigenvalues crosses the imaginary axis along the real axis from the left-half-plane to the right-half-plane. Instead, one stable solution of the third symmetric mode grows rapidly all the way. Moreover, the other stable solutions of the first and third symmetric mode decrease as σ_2 increases. We can also note that the amplitude of the third symmetric mode tends to zero for the large value of σ_2, which means that the third symmetric mode seems to be very difficult to be activated.

The effects of the elasto-geometric parameter λ on the frequency-response curves are investigated. In this case, λ is reduced to 1.43π, and the detuning parameter σ_1 becomes 0.5. The frequency–force curves for the primary resonance of the first symmetric mode with $\mu_1 = 0.05$, $\mu_2 = 0.01$, $f_1 = 0.16$ and $\sigma_1 = 0.5$ are shown in Fig. 5. Compared with Fig. 4, we can note that the amplitude of the third symmetric mode decreases but the amplitude of the first symmetric mode increases as σ_1 increases or λ decreases. Referring to Table 1, we can also note that the absolute value of the nonlinear interaction coefficients decreases as the elasto-geometric parameter λ decreases. Therefore, we can conclude that the strength of the modal interaction due to three-to-one internal resonances decreases as λ decreases. Moreover, another significant difference of the frequency-response curves is the disappearance of the mutation of the first symmetric mode's amplitude.

The force-response curves for $\mu_1 = 0.05$, $\mu_2 = 0.01$, $\sigma_1 = -1.5$ and $\sigma_2 = -1.75$ are shown in Fig. 6, where HB represents the Hopf bifurcation point. The force-response curves exhibit a relatively small multi-valued range due to the saddle-node bifurcations at SN1 and SN2. As f_1 increases from 0.092, one stable solution loses its stability via the Hopf bifurcation at HB1, where one pair of complex conjugate eigenvalues crosses the imaginary axis transversely from the left- to the right-half-plane. Following, the unstable solution regains its stability via the reverse Hopf bifurcation, indicated by HB2 in Fig. 6.

4.2. Primary resonance of the third symmetric mode

In this case, there are two possibilities: first $a_1 = 0$, $a_3 \neq 0$; second $a_1 \neq 0$, $a_3 \neq 0$. For the first case, a_3 and γ_2 are determined by

$$\mu_2 a_3 = \frac{f_3}{2\omega_3} \sin \gamma_2, \tag{58}$$

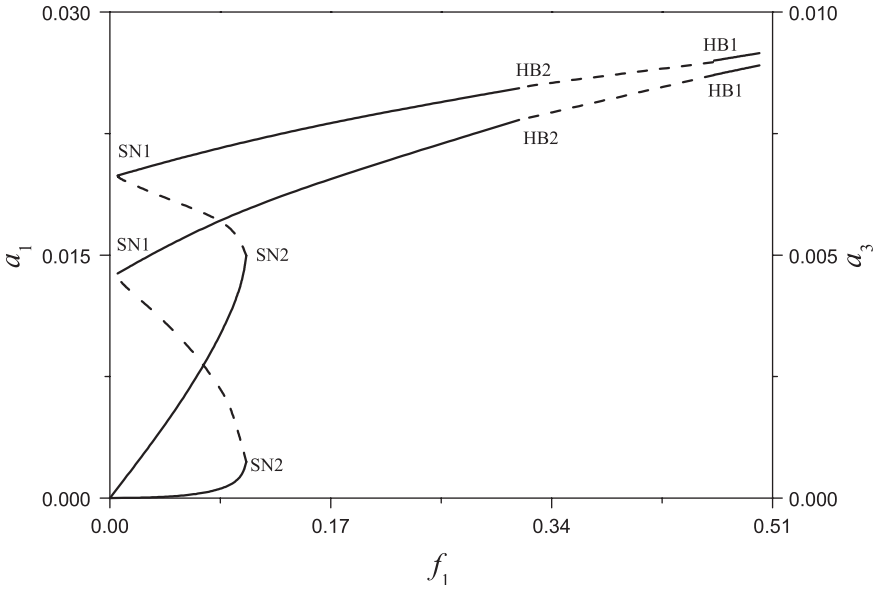

Fig. 6. Force-response curves for the primary resonance of the first symmetric mode: $\mu_1 = 0.05$, $\mu_2 = 0.01$, $\sigma_1 = -1.5$ and $\sigma_2 = -1.75$.

$$\sigma_2 a_3 = -\frac{\Gamma_{22}}{8\omega_3} a_3^3 - \frac{f_3}{2\omega_3} \cos\gamma_2. \tag{59}$$

Hence, the frequency-response equation is given by

$$\sigma_2 = -\frac{\Gamma_{22}}{8\omega_3} a_3^2 \pm \left(\frac{f_3^2}{4\omega_3^2 a_3^2} - \mu_2^2\right)^{1/2}, \tag{60}$$

or we can obtain a_3 through the relation $a_3 = \sqrt{p_3^2 + q_3^2}$ by using the following equations:

$$\mu_2 p_3 = -\sigma_2 q_3 - \frac{1}{8\omega_3} \{\Gamma_{22} q_3 (p_3^2 + q_3^2)\}, \tag{61}$$

$$\mu_2 q_3 = \sigma_2 p_3 - \frac{1}{8\omega_3} \{\Gamma_{22} p_3 (p_3^2 + q_3^2)\} + \frac{f_3}{2\omega_3}. \tag{62}$$

In general, the single-mode response can be determined by Eqs. (58) and (59) or Eqs. (61) and (62). However, the stability of the single-mode solution must be ascertained by the corresponding eigenvalues of the Jacobian matrix of Eqs. (53)–(56). For the second case, we can determine the equilibrium solutions and their stability by using the usual procedure.

Fig. 7 shows the frequency-response curves for the primary resonance of the third symmetric mode when $\mu_1 = 0.05$, $\mu_2 = 0.01$, $\sigma_1 = -1.5$ and $f_3 = 0.50$. The single-mode response exhibits a hardening behavior, which is due to the fact that the *effective nonlinearity coefficient* [20] Γ_{22} is negative (see Table 1). It should be pointed out that, when $\lambda < 3.5\pi$ (excepting very small value of λ), the *effective nonlinearity coefficient* is positive for the first symmetric mode [20], and is negative for the higher symmetric mode [25] (e.g. the third symmetric mode). Furthermore, a saddle-node bifurcation of the single-mode solution occurs at $\sigma_2 = 4.721$.

When σ_2 is very small, Fig. 7 shows that there are four branches of the two-mode solutions, which end at the two saddle-node bifurcations (SN1, SN2). All the two-mode solution branches are isolated from the single-mode solution, although the saddle-node bifurcation point SN2 is very close to the single-mode solution branch. Similar to this case, the isolated two-mode solution branches were also found in the hinged-clamped beam with the three-to-one internal resonance excited by primary resonance of higher mode [26]. Moreover, as

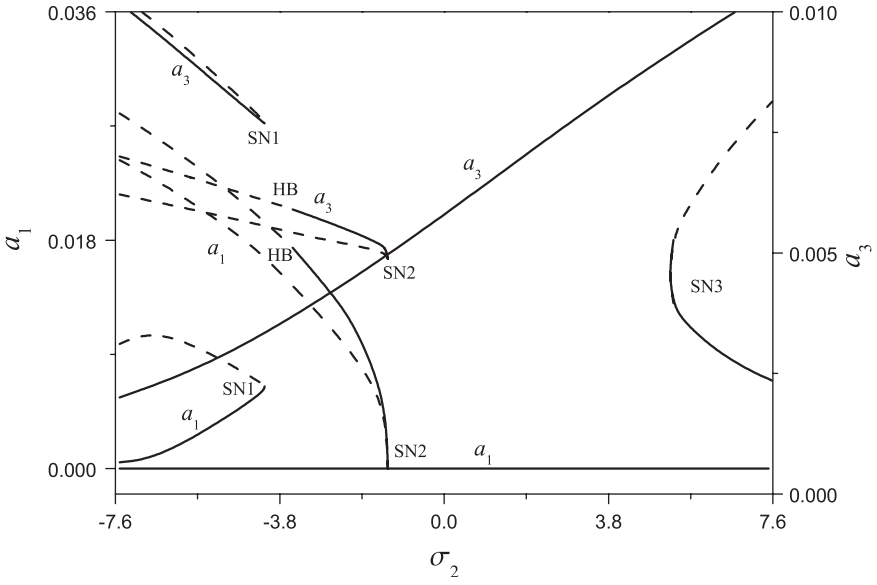

Fig. 7. Frequency-response curves for the primary resonance of the third symmetric mode: $\mu_1 = 0.05$, $\mu_2 = 0.01$, $\sigma_1 = -1.5$ and $f_3 = 0.50$.

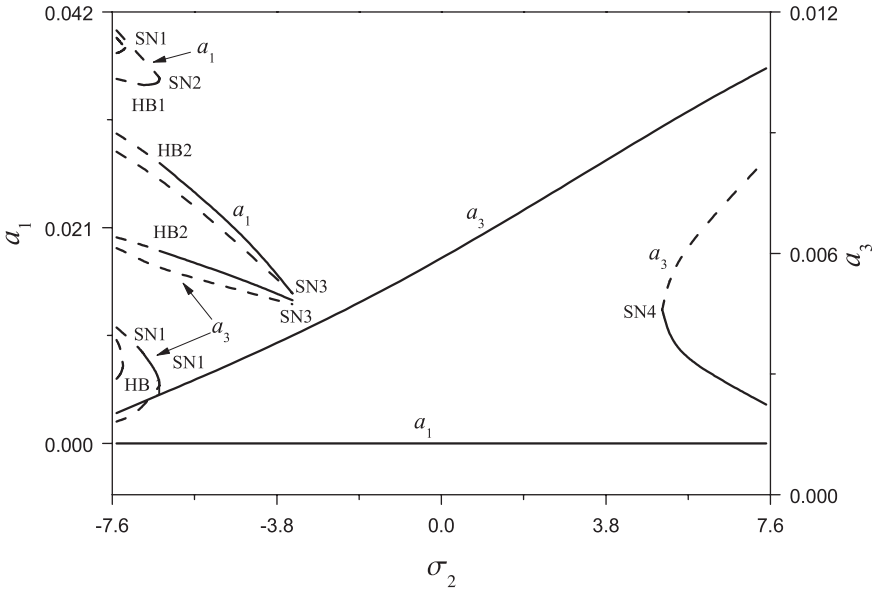

Fig. 8. Frequency-response curves for the primary resonance of the third symmetric mode: $\mu_1 = 0.05$, $\mu_2 = 0.01$, $\sigma_1 = 0.5$ and $f_3 = 0.50$.

σ_2 decreases from -1.43, the stable two-mode solutions are found to undergo a supercritical Hopf bifurcation at HB, giving rise to periodic solution with period $2\pi/|\beta|$, where β is the purely imaginary eigenvalue.

Next, the effects of the detuning parameter σ_1 or the elasto-geometric parameter λ on the frequency-response curves for the primary resonance of the third symmetric mode are shown in Fig. 8 when $\mu_1 = 0.05$, $\mu_2 = 0.01, f_3 = 0.50$ and $\sigma_1 = 0.5$. Figs. 7 and 8 show that the amplitude of the directly excited high-frequency mode decreases and the amplitude of the indirectly excited low-frequency mode increases when σ_1 increases. Fig. 8 also shows that there exist two-mode equilibrium solution branches when $\sigma_2 < -7.25$ in the present case.

5. Dynamic solutions

According to the Hopf bifurcation theorem [24,27], a small limit cycle is born in the phase-plane as a result of the Hopf bifurcation. The limit cycle is stable if the bifurcation is supercritical, and unstable if the bifurcation is subcritical. In this section, the periodic solution and chaotic solution of the modulation equations are investigated. Because the Cartesian form of the modulation equations has the standard form as

$$\dot{\mathbf{x}} = \mathbf{F}(\mathbf{x}), \tag{63}$$

it is used to examine the dynamic solution by applying the shooting method [24]. And the stability of the periodic solution is determined by using the Floquet theory [24]. Then the pseudo-arclength path following algorithm can be used to trace the periodic solution branch. In the following figures, the open circles denote the unstable periodic solutions, and the filled circles denote the stable periodic solutions.

5.1. Primary resonance of the first symmetric mode

On continuing the periodic solutions emerging from HB1 and HB2 in Fig. 6, Fig. 9 shows the periodic solutions of the modulation equations as the functions of f_1 with $\mu_1 = 0.05$, $\mu_2 = 0.01$, $\sigma_1 = -1.5$ and $\sigma_2 = -1.75$, and TR represents the torus bifurcation point. It is observed from Fig. 9 that the two Hopf bifurcations (HB1 and HB2) are subcritical, due to the fact that the periodic solution are unstable. Following branch I, the periodic solution undergoes a secondary Hopf bifurcation (Neimark–Sacker bifurcation) at $f_1 = 0.0325$, leading to a unstable torus. To illustrate the torus, Fig. 10 shows the time history of one representative torus with $f_1 = 0.032$. Note that the unstable periodic orbit, with period $T \approx 6$, composes the main part of the motion, and the small amplitude wiggles are caused by the second frequency. As f_1 decreases, we can obtain a sequence of torus bifurcations.

Because the Hopf bifurcation is subcritical, the post-bifurcation behavior of the modulation equations cannot be determined by local analysis. Moreover, the torus bifurcation is far from the Hopf bifurcation

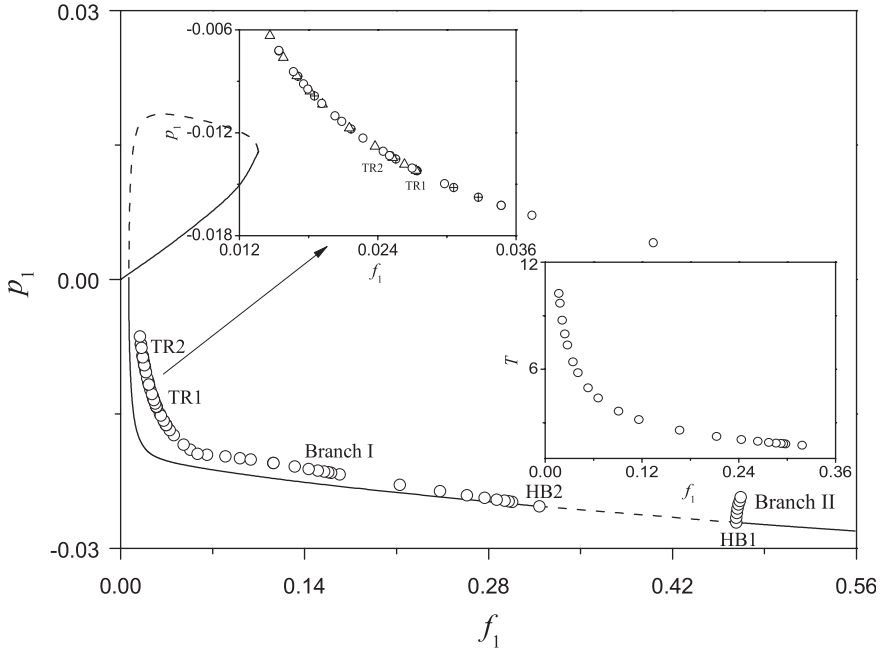

Fig. 9. The periodic solutions and the time-period of the P-1 solution for the primary resonance of the first symmetric mode: $\mu_1 = 0.05$, $\mu_2 = 0.01$, $\sigma_1 = -1.5$ and $\sigma_2 = -1.75$.

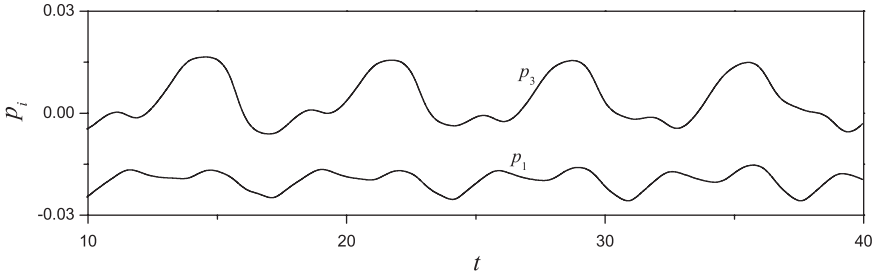

Fig. 10. The time history of a torus at $f_1 = 0.032$: $\mu_1 = 0.05$, $\mu_2 = 0.01$, $\sigma_1 = -1.5$ and $\sigma_2 = -1.75$.

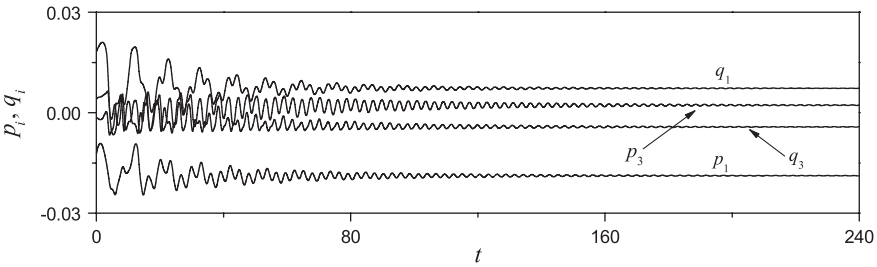

Fig. 11. The time history of the modulation equations at $f_1 = 0.0175$: $\mu_1 = 0.05$, $\mu_2 = 0.01$, $\sigma_1 = -1.5$ and $\sigma_2 = -1.75$.

point, which occurs on the nontrivial states. Therefore, we do not expect any interactions between these two bifurcations. To better understand the motion of the torus, the modulation equations are numerically integrated by using the four-order Runge–Kutta numerical algorithm, whose initial conditions are set to the ones obtained by the modulation equations. Fig. 11 shows the long time history of the modulation equations. We can note that this sequence of torus bifurcations cannot lead to chaos, whereas, the unstable torus jumps to the stable equilibrium solution, which is mainly due to the fact that these periodic solutions are all unstable.

Moreover, the time-period (T) of the periodic solution starting from HB1 as the function of the parameter f_1 is also included in Fig. 9. We can also note that the period increases rapidly when f_1 decreases. Furthermore, another unstable periodic solution branch (Branch II) starting from HB2 terminates immediately at $f_1 = 0.468$.

Next, the effects of the damping parameter μ_2 on the periodic solution are investigated. Fig. 12 shows the periodic solution and its time-period (T) as the functions of f_1 with $\mu_1 = 0.05$, $\mu_2 = 0.05$, $\sigma_1 = -1.5$ and $\sigma_2 = -1.75$. Starting from the subcritical Hopf bifurcation, the unstable periodic solution continues along the equilibrium solution and terminates at the saddle S which lies on the unstable equilibrium solution branch. And we can also note that the period T of the unstable periodic solution increases rapidly and tends to ∞, which indicates that the periodic orbit is close to the homoclinic orbit [27]. Choosing the parameter $f_1 = 0.0152$ with the maximum period T, we obtain an approximate homoclinic orbit as shown in Fig. 13.

5.2. Primary resonance of the third symmetric mode

Choosing the HB point in Fig. 7 as the initial point, we obtain the periodic solution branch for $\mu_1 = 0.05$, $\mu_2 = 0.01$, $\sigma_1 = -1.5$ and $f_3 = 0.50$, as shown in Fig. 14, where PD represents the period-doubling bifurcation point. The period-1 solution (P-1) is stable over the detuning interval $\sigma_2 \in (-4.41, -3.45)$, and loses its stability via the period-doubling bifurcation, indicated by PD in Fig. 14. On continuing the period-2 solution

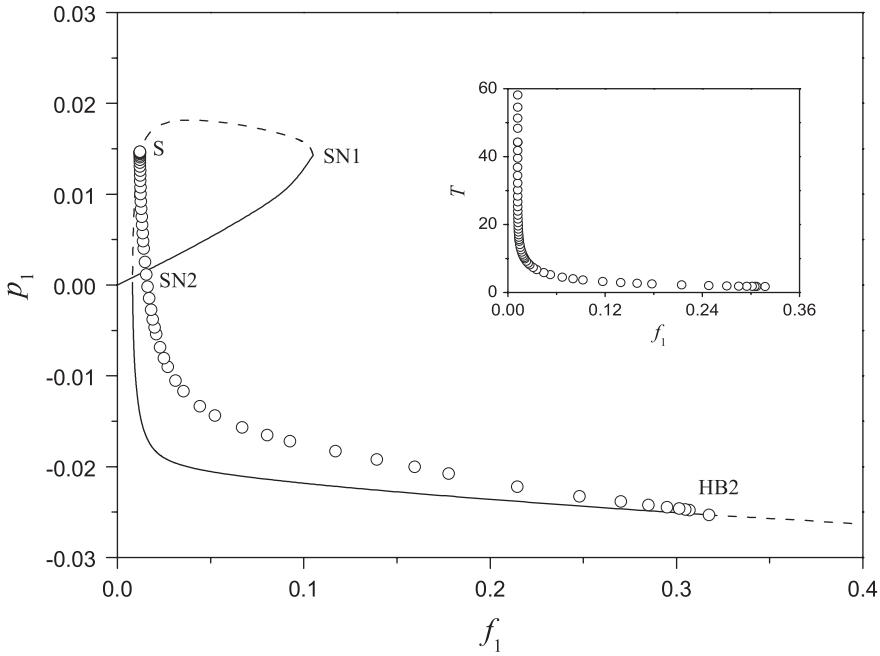

Fig. 12. The periodic solutions and the time-period of the period-1 solution for the primary resonance of the first symmetric mode: $\mu_1 = 0.05$, $\mu_2 = 0.05$, $\sigma_1 = -1.5$ and $\sigma_2 = -1.75$.

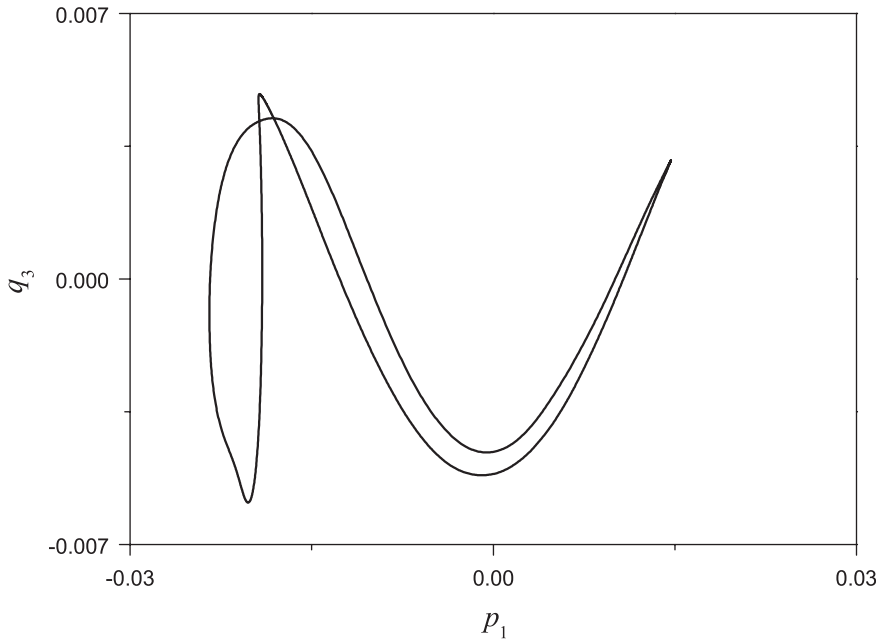

Fig. 13. Approximate homoclinic orbit at $f_1 = 0.0152$: $\mu_1 = 0.05$, $\mu_2 = 0.05$, $\sigma_1 = -1.5$ and $\sigma_2 = -1.75$.

(P-2) branch emerging from PD, we can obtain a cascade of period-doubling bifurcations, which eventually leads to chaos. The time-period (T) of the periodic solution as the function of the detuning parameter σ_2 is also included in Fig. 14, which shows that the variation of period is very small.

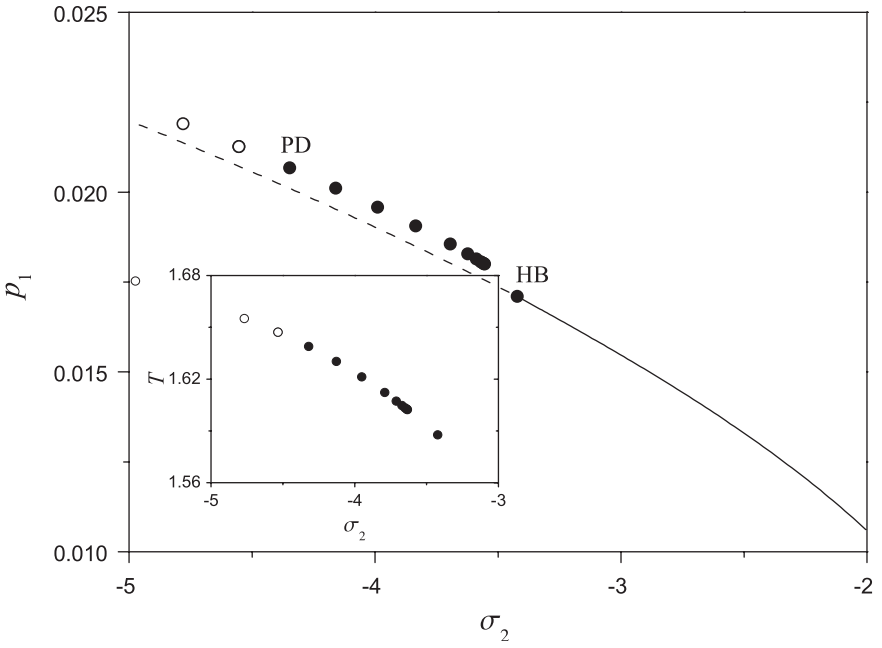

Fig. 14. The periodic solutions and the time-period of the P-1 solution for the primary resonance of the third symmetric mode: $\mu_1 = 0.05$, $\mu_2 = 0.01$, $\sigma_1 = -1.5$ and $f_3 = 0.50$.

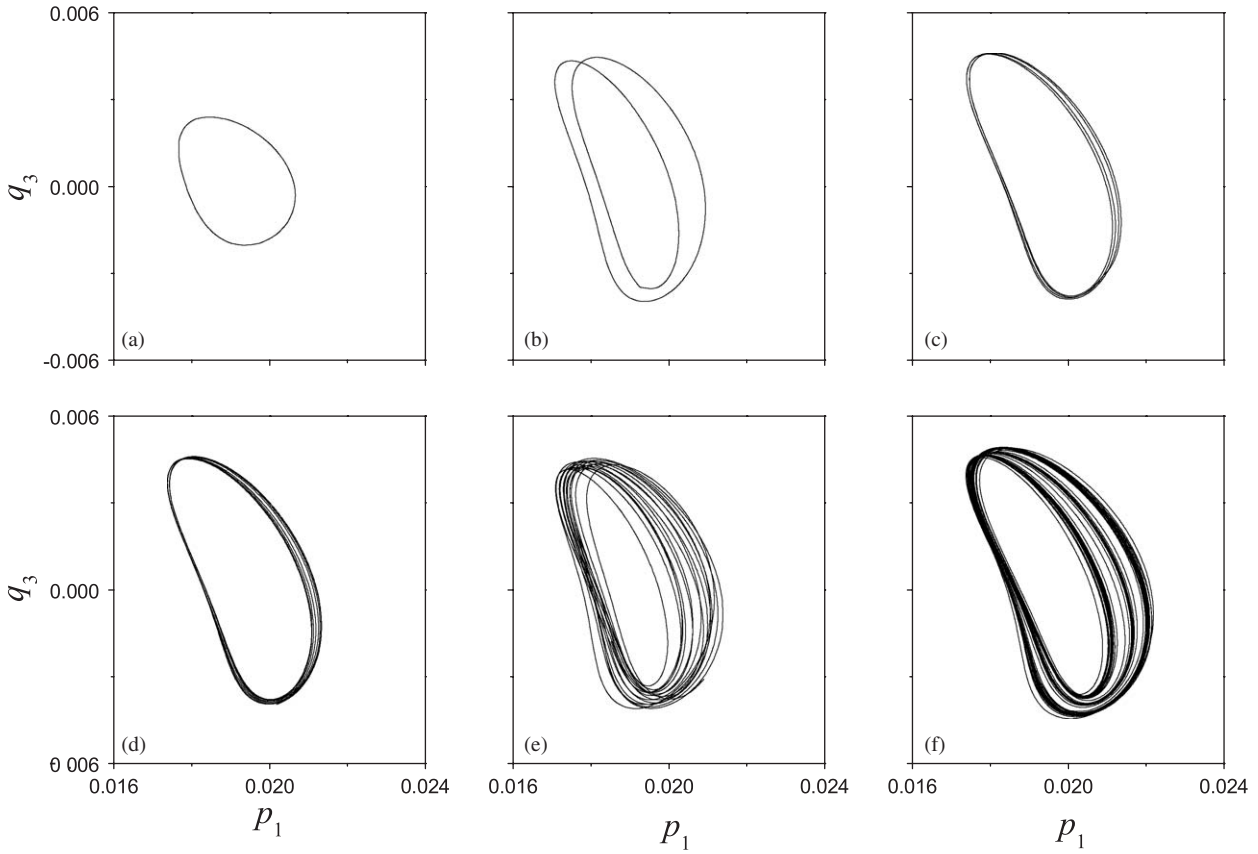

Fig. 15. Two-dimensional projections of phase portraits onto $(p_1 - q_3)$ phase space for $\mu_1 = 0.05$, $\mu_2 = 0.01$, $\sigma_1 = -1.5$ and $f_3 = 0.50$: (a) $\sigma_2 = -4.4$(P-1); (b) $\sigma_2 = -4.54$(P-2); (c) $\sigma_2 = -4.542$(P-4); (d) $\sigma_2 = -4.543$(P-8); (e) $\sigma_2 = -4.545$(P-16); (f) $\sigma_2 = -4.547$ (chaos).

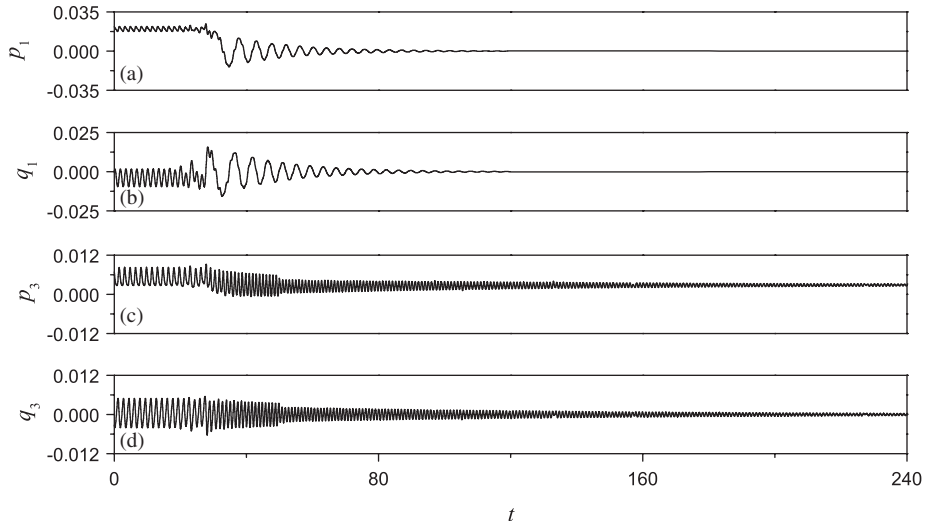

Fig. 16. The time history of the modulation equations at $\sigma_2 = -4.549$ after a crisis occurs.

Then, it is numerically demonstrated that the modulation equations exhibit a cascade of period-doubling bifurcations leading to chaos. Fig. 15 shows two-dimensional projections of the phase portraits onto the $p_1 - q_3$ plane as the detuning parameter σ_2 slowly varies. When σ_2 increases past the Hopf bifurcation point (HB1), a small limit cycle is born, as shown in Fig. 15a. As σ_2 decreases, the limit cycle undergoes a cascade of period-doubling bifurcations at $\sigma_2 = -4.54$(P-2), $\sigma_2 = -4.542$(P-4), $\sigma_2 = -4.543$(P-8), $\sigma_2 = -4.545$(P-16). It may be noted that this cascade of period-doubling values converges quickly to a value around $\sigma_2 = -4.546$. At last the cascade of period-doubling bifurcations leads to chaos. Fig. 15f shows one representative chaotic attractor for $\sigma_2 = -4.547$. As σ_2 decreases further, the chaotic attractor encounters a boundary crisis. Fig. 16 shows the time history of the modulation equations after the boundary crisis occurs. Referring to Fig. 16, we can note that the chaotic attractor only lasts a finite long *chaotic transients* time, then settles down to the stable single-mode equilibrium solution. Here, it is worth mentioning that the investigation of Chin and Nayfeh [26] on the dynamic solution of the hinged-clamped beams with three-to-one internal resonances is similar to the present case. They also numerically demonstrated that the P-1 solution undergoes a sequence of period-doubling bifurcations leading to chaos.

In Fig. 17, we show the variation of the dynamic configurations over one period of vibration when $\lambda = 1.57\pi$, where the dashed line denotes the initial deflection, and the solid line denotes the current dynamic configuration. We can note that the shapes of functions $\Psi_i(x)$ (see Fig. 3) play a dominant role on the spatial configurations of the suspended cable.

6. Conclusion

The two-mode response of the suspended cable subjected to the primary resonance is examined. As examples, the primary resonance of the first symmetric mode and the primary resonance of the third symmetric mode are investigated. The method of multiple scales is used to directly attack the equation of motion and the boundary conditions, which leads to four first-order nonlinear ordinary-differential equations describing the modulation of the amplitude and phases of the interaction modes.

Then the Newton–Raphson method is used to determine the equilibrium solution, whose stability is determined by examining the eigenvalues of the corresponding Jacobian matrix.

Also the dynamic solution of the modulation equations is obtained by the shooting method. And the Folquet theory is applied to determine the stability of the dynamic solution. Some complex nonlinear dynamics phenomena, including torus bifurcation, period-doubling bifurcations, boundary crisis, and chaos, are investigated.

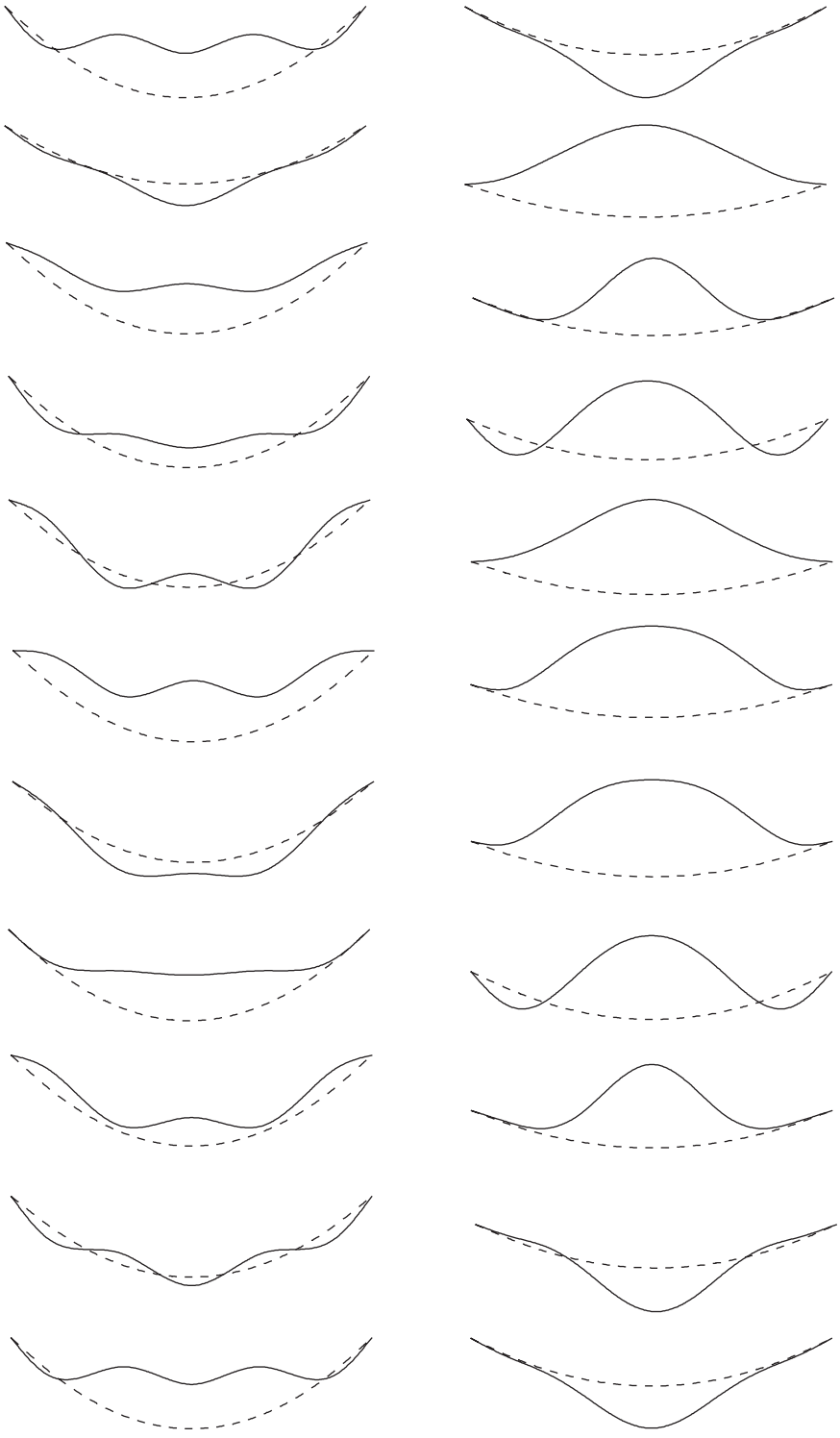

Fig. 17. In-plane displacement field for the two-mode solution: the first column—the primary resonance of the first symmetric mode with $\sigma_2 = -5.5$, the second column—the primary resonance of the third symmetric mode $\sigma_2 = -3.0$, other parameters see Figs. 4 and 7. The dashed line denotes the initial deflection, and the solid line denotes the current dynamic configuration.

Acknowledgement

The study was supported by National Science Foundation of China under Grant No. 10272041 and 10502020. Interesting comments and criticism by the reviewers are also gratefully acknowledged.

Appendix A

$$\Pi_1 = \alpha\phi_1'' \int_0^1 \phi_1' y' \,\mathrm{d}x + \frac{1}{2}\alpha y'' \int_0^1 \phi_1' \phi_1' \,\mathrm{d}x, \tag{64}$$

$$\Pi_2 = \alpha\phi_3'' \int_0^1 \phi_3' y' \,\mathrm{d}x + \frac{1}{2}\alpha y'' \int_0^1 \phi_3' \phi_3' \,\mathrm{d}x, \tag{65}$$

$$\Pi_3 = \alpha\phi_1'' \int_0^1 \phi_3' y' \,\mathrm{d}x + \alpha y'' \int_0^1 \phi_1' \phi_3' \,\mathrm{d}x + \alpha\phi_3'' \int_0^1 \phi_1' y' \,\mathrm{d}x, \tag{66}$$

$$\Pi_4 = \alpha\phi_1'' \int_0^1 \phi_3' y' \,\mathrm{d}x + \alpha y'' \int_0^1 \phi_1' \phi_3' \,\mathrm{d}x + \alpha\phi_3'' \int_0^1 \phi_1' y' \,\mathrm{d}x, \tag{67}$$

$$\Pi_5 = \alpha\phi_1'' \int_0^1 \phi_1' y' \,\mathrm{d}x + \frac{1}{2}\alpha y'' \int_0^1 \phi_1' \phi_1' \,\mathrm{d}x, \tag{68}$$

$$\Pi_6 = \alpha\phi_3'' \int_0^1 \phi_3' y' \,\mathrm{d}x + \frac{1}{2}\alpha y'' \int_0^1 \phi_3' \phi_3' \,\mathrm{d}x, \tag{69}$$

$$\begin{aligned}\chi_1(x) = {} & \alpha\phi_1'' \int_0^1 \Psi_1' y' \,\mathrm{d}x + \alpha y'' \int_0^1 \phi_1' \Psi_1' \,\mathrm{d}x + \alpha\Psi_1'' \int_0^1 \phi_1' y' \,\mathrm{d}x \\ & + 2\alpha\phi_1'' \int_0^1 \Psi_5' y' \,\mathrm{d}x + 2\alpha y'' \int_0^1 \phi_1' \Psi_5' \,\mathrm{d}x + 2\alpha\Psi_5'' \int_0^1 \phi_1' y' \,\mathrm{d}x \\ & + \frac{3}{2}\alpha\phi_1'' \int_0^1 \phi_1' \phi_1' \,\mathrm{d}x,\end{aligned} \tag{70}$$

$$\begin{aligned}\chi_2(x) = {} & \alpha\phi_3'' \int_0^1 \Psi_3' y' \,\mathrm{d}x + \alpha y'' \int_0^1 \phi_3' \Psi_3' \,\mathrm{d}x + \alpha\Psi_3'' \int_0^1 \phi_3' y' \,\mathrm{d}x \\ & + \alpha\phi_3'' \int_0^1 \Psi_4' y' \,\mathrm{d}x + \alpha y'' \int_0^1 \phi_3' \Psi_4' \,\mathrm{d}x + \alpha\Psi_4'' \int_0^1 \phi_3' y' \,\mathrm{d}x \\ & + 2\alpha\phi_1'' \int_0^1 \Psi_6' y' \,\mathrm{d}x + 2\alpha y'' \int_0^1 \phi_3' \Psi_6' \,\mathrm{d}x + 2\alpha\Psi_6'' \int_0^1 \phi_1' y' \,\mathrm{d}x \\ & + \alpha\phi_3'' \int_0^1 \phi_3' \phi_1' \,\mathrm{d}x + \alpha\phi_3'' \int_0^1 \phi_1' \phi_3' \,\mathrm{d}x + \alpha\phi_1'' \int_0^1 \phi_3' \phi_3' \,\mathrm{d}x,\end{aligned} \tag{71}$$

$$\begin{aligned}\chi_3(x) = {} & \alpha\phi_3'' \int_0^1 \Psi_1' y' \,\mathrm{d}x + \alpha y'' \int_0^1 \phi_3' \Psi_1' \mathrm{d}x + \alpha\Psi_1'' \int_0^1 \phi_3' y' \,\mathrm{d}x \\ & + \alpha\phi_1'' \int_0^1 \Psi_4' y' \,\mathrm{d}x + \alpha y'' \int_0^1 \phi_1' \Psi_4' \,\mathrm{d}x + \alpha\Psi_4'' \int_0^1 \phi_1' y' \,\mathrm{d}x \\ & + \frac{1}{2}\alpha\phi_3'' \int_0^1 \phi_1' \phi_1' \,\mathrm{d}x + \frac{1}{2}\alpha\phi_1'' \int_0^1 \phi_1' \phi_3' \,\mathrm{d}x + \frac{1}{2}\alpha\phi_1'' \int_0^1 \phi_3' \phi_1' \,\mathrm{d}x,\end{aligned} \tag{72}$$

$$\chi_4(x) = \alpha\phi_1'' \int_0^1 \Psi_3' y' \,\mathrm{d}x + \alpha y'' \int_0^1 \phi_1' \Psi_3' \,\mathrm{d}x + \alpha\Psi_3'' \int_0^1 \phi_1' y' \,\mathrm{d}x + \alpha\phi_1'' \int_0^1 \Psi_4' y' \,\mathrm{d}x + \alpha y'' \int_0^1 \phi_1' \Psi_4' \,\mathrm{d}x + \alpha\Psi_4'' \int_0^1 \phi_1' y' \,\mathrm{d}x + 2\alpha\phi_3'' \int_0^1 \Psi_5' y' \,\mathrm{d}x + 2\alpha y'' \int_0^1 \phi_1' \Psi_5' \,\mathrm{d}x + 2\alpha\Psi_5'' \int_0^1 \phi_3' y' \,\mathrm{d}x + \alpha\phi_1'' \int_0^1 \phi_1' \phi_3' \,\mathrm{d}x + \alpha\phi_3'' \int_0^1 \phi_1' \phi_1' \,\mathrm{d}x + \alpha\phi_1'' \int_0^1 \phi_3' \phi_1' \,\mathrm{d}x, \tag{73}$$

$$\chi_5(x) = \alpha\phi_3'' \int_0^1 \Psi_2' y' \,\mathrm{d}x + \alpha y'' \int_0^1 \phi_3' \Psi_2' \,\mathrm{d}x + \alpha\Psi_2'' \int_0^1 \phi_3' y' \,\mathrm{d}x + 2\alpha\phi_3'' \int_0^1 \Psi_6' y' \,\mathrm{d}x + 2\alpha y'' \int_0^1 \phi_3' \Psi_6' \,\mathrm{d}x + 2\alpha\Psi_6'' \int_0^1 \phi_3' y' \,\mathrm{d}x + \frac{3}{2}\alpha\phi_3'' \int_0^1 \phi_3' \phi_3' \,\mathrm{d}x, \tag{74}$$

$$\chi_6(x) = \alpha\phi_1' \int_0^1 \Psi_1' y' \,\mathrm{d}x + \alpha y'' \int_0^1 \phi_1' \Psi_1' \,\mathrm{d}x + \alpha\Psi_1' \int_0^1 \phi_1' y' \,\mathrm{d}x + \frac{1}{2}\alpha\phi_1'' \int_0^1 \phi_1' \phi_1' \,\mathrm{d}x, \tag{75}$$

$$\mu_1 = \int_0^1 c(x)\phi_1^2(x) \,\mathrm{d}x \quad \text{and} \quad \mu_2 = \int_0^1 c(x)\phi_3^2(x) \,\mathrm{d}x, \tag{76}$$

$$f_1 = \int_0^1 F(x)\phi_1(x) \,\mathrm{d}x \quad \text{and} \quad f_3 = \int_0^1 F(x)\phi_3(x) \,\mathrm{d}x, \tag{77}$$

$$\Gamma_{11} = \int_0^1 \chi_1(x)\phi_1(x) \,\mathrm{d}x, \quad \Gamma_{12} = \int_0^1 \chi_2(x)\phi_1(x) \,\mathrm{d}x, \quad \Gamma_{13} = \int_0^1 \chi_3(x)\phi_1(x) \,\mathrm{d}x,$$

$$\Gamma_{21} = \int_0^1 \chi_4(x)\phi_3(x) \,\mathrm{d}x, \quad \Gamma_{22} = \int_0^1 \chi_5(x)\phi_3(x) \,\mathrm{d}x, \quad \Gamma_{23} = \int_0^1 \chi_6(x)\phi_3(x) \,\mathrm{d}x. \tag{78}$$

References

[1] M.S. Triantafyllou, Dynamics of cables, towing cables, and mooring systems, *Shock and Vibration Digest* 23 (1991) 3–8.

[2] H.M. Irvine, T.K. Caughey, The linear theory of free vibrations of a suspended cable, *Proceeding of the Royal Society of London A* 341 (1974) 299–315.

[3] H.M. Irvine, *Cable Structures*, The MIT Press, Cambridge, 1981.

[4] P. Hagedon, B. Schäfer, On non-linear free vibrations of an elastic cables, *International Journal of Non-linear Mechanics* 15 (1980) 333–339.

[5] A. Luongo, G. Rega, F. Vestroni, Planar non-linear free vibrations of an elastic cable, *International Journal of Non-linear Mechanics* 19 (1984) 39–52.

[6] F. Benedettini, G. Rega, Non-linear dynamics of an elastic cable under planar excitation, *International Journal of Non-linear Mechanics* 22 (1987) 497–509.

[7] F. Benedettini, G. Rega, F. Vestroni, Modal coupling in the free nonplanar finite motion of an elastic cable, *Meccanica* 21 (1986) 38–46.

[8] G.V. Rao, R.N. Iyengar, Internal resonance and non-linear response of a cable under periodic excitation, *Journal of Sound and Vibration* 149 (1991) 25–41.

[9] N.C. Perkins, Modal interactions in the non-linear response of elastic cables under parametric/external excitation, *International Journal of Non-linear Mechanics* 27 (1992) 233–250.
[10] C.L. Lee, N.C. Perkins, Non-linear oscillations of suspended cables containing a two-to-one internal resonance, *Nonlinear Dynamics* 3 (1993) 465–490.
[11] C.L. Lee, N.C. Perkins, Three-dimensional oscillations of suspended cables involving simultaneous internal resonances, *Nonlinear Dynamics* 8 (1995) 45–63.
[12] M. Pakdemirli, S.A. Nayfeh, A.H. Nayfeh, Analysis of one-to-one autoparametric resonances in cables: discretization versus direct treatment, *Nonlinear Dynamics* 8 (1995) 65–83.
[13] F. Benedettini, G. Rega, R. Alaggio, Non-linear oscillations of a four-degree-of-freedom model of a suspended cable under multiple internal resonance conditions, *Journal of Sound and Vibration* 182 (1995) 775–798.
[14] G. Rega, R. Alaggio, F. Benedettini, Experimental investigation of the non-linear response of a hanging cable. Part I: local analysis, *Nonlinear Dynamics* 14 (1997) 89–117.
[15] G. Rega, W. Lacarbonara, A.H. Nayfeh, C.-M. Chin, Multiple resonances in suspended cables: direct versus reduced-order models, *International Journal of Non-linear Mechanics* 34 (1999) 901–924.
[16] A.H. Nayfeh, A.H. Arafat, C.-M. Chin, W. Lacarbonara, Multimode interactions in suspended cables, *Journal of Vibration and Control* 8 (2002) 337–387.
[17] Y.Y. Zhao, L.H. Wang, D.L. Chen, L.Z. Jiang, Nonlinear dynamic analysis of the two-dimensional simplified model of an elastic cable, *Journal of Sound and Vibration* 255 (2002) 43–59.
[18] N. Srinil, G. Rega, S. Chucheepsakul, Large amplitude three-dimensional free vibration of inclined sagged elastic cable, *Nonlinear Dynamics* 33 (2003) 129–154.
[19] W. Lacarbonara, G. Rega, Resonat non-linear normal modes. Part II: activation/orthogonality conditions for shallow structural systems, *International Journal of Non-linear Mechanics* 38 (2003) 873–887.
[20] G. Rega, W. Lacarbonara, A.H. Nayfeh, Reduction methods for nonlinear vibrations of spatially continuous systems with initial curvature, in: N. Van Dao, E.J. Kreuzer (Eds.), *Proceedings of the IUTAM Symposium on Recent Developments in Non-linear Oscillations of Mechanical Systems, Solid Mechanics its Application*, Vol. 77, 2000, pp. 235–246.
[21] A.H. Nayfeh, *Non-linear Interactions*, Wiley-Interscience, New York, 2000.
[22] W. Lacarbonara, G. Rega, A.H. Nayfeh, Resonant non-linear normal modes. Part I: analytical treatment for structural one-dimensional systems, *International Journal of Non-linear Mechanics* 38 (2003) 851–871.
[23] A.H. Nayfeh, D.T. Mook, *Nonlinear Oscillations*, Wiley-Interscience, New York, 1979.
[24] A.H. Nayfeh, B. Balachandran, *Applied Nonlinear Dynamics*, Wiley-Interscience, New York, 1994.
[25] Y.Y. Zhao, L.H. Wang, W.C. Liu, H.B. Zhou, Direct treatment and discretizations of non-linear dynamics of suspended cables, *Acta Mechanica Sinica* 37 (2005) 329–339 (in Chinese).
[26] C.-M. Chin, A.H. Nayfeh, Three-to-one internal resonances in hinged-clamped beams, *Nonlinear Dynamics* 12 (1997) 129–154.
[27] R. Seydel, *Practical Bifurcation and Stability Analysis: From Equilibrium to Chaos*, Springer, Berlin, 1999.